

Interfacial friction based quasi-continuum hydrodynamical model for nanofluidic transport of water

Ravi Bhaduria, Tarun Sanghi, and N. R. Aluru^{a)}

Department of Mechanical Science and Engineering, Beckman Institute for Advanced Science and Technology, University of Illinois at Urbana-Champaign, Urbana, Illinois 61801, USA

(Received 15 July 2015; accepted 15 October 2015; published online 3 November 2015)

In this work, we formulate a one-dimensional isothermal hydrodynamic transport model for water, which is an extension to our recently proposed hydrodynamic model for Lennard-Jones type fluid [R. Bhaduria and N. R. Aluru, *J. Chem. Phys.* **139**, 074109 (2013)]. Viscosity variations in confinement are incorporated by the local average density method. Dirichlet boundary conditions are provided in the form of slip velocity that depends upon the macroscopic interfacial friction coefficient. The value of this friction coefficient is computed using a novel generalized Langevin equation formulation that eliminates the use of equilibrium molecular dynamics simulation. Gravity driven flows of SPC/E water confined between graphene and silicon slit shaped nanochannels are considered as examples for low and high friction cases. The proposed model yields good quantitative agreement with the velocity profiles obtained from non-equilibrium molecular dynamics simulations. © 2015 AIP Publishing LLC. [<http://dx.doi.org/10.1063/1.4934678>]

I. INTRODUCTION

Understanding the behavior of water with different reagents, chemicals, and surfaces is imperative due to its role in biological and industrial processes. With the growing impetus of nanotechnology research, physics of confined water has generated tremendous curiosity, ranging from studying naturally occurring transmembrane protein channels like aquaporins^{1,2} to artificially manufactured graphene/graphite slits and Carbon Nano-Tubes (CNT).^{3–11} The potential applications include water purification,^{11–14} biological flows in membranes,^{1,2,15} energy harvesting,¹⁶ and many others. These applications have instigated the need to understand the fundamental mechanism of water transport under confinement, both from experimental and theoretical standpoint.¹⁷

The nature of interaction between the surface and the fluid is central to understand the flow physics,^{18–20} and it affects the flow in two different ways. First, competing surface and fluid interactions result in structural inhomogeneity of the fluid.^{21–25} This structural inhomogeneity leads to spatially inhomogeneous viscosity.^{26–30} Viscous contribution is dominant for flows in naturally occurring hydrophilic channels such as silicates.^{31,32} Second, the lattice structure and the chemical properties of the surface could result in the motion of the fluid molecules relative to the surface, a phenomenon more commonly known as slip.^{33–36} Several experimental^{3–6} and Molecular Dynamics (MD)^{7–9,11} studies have reported high enhancement, slip dominant flow in engineered hydrophobic surfaces. Therefore, an accurate account of both of these phenomena is critical for the development of a transport model for confined fluids.¹⁷ Several models incorporating viscous and slip phenomena exist; among those a few focus on the specific cases of low adsorbed densities in the nanochannel,

where the structural inhomogeneity does not play a major role.^{37–40} Another class of models overlooks the viscosity inhomogeneity by focusing only on slip dominant flows.^{41,42}

A general slip boundary condition for hydrodynamics prevalent in the literature is given as

$$l_s \left. \frac{du_x(z)}{dz} \right|_{z=\delta} = u_s, \quad (1)$$

where z is the direction perpendicular to the confining walls, u_x is the velocity field, l_s is the slip length, du_x/dz is the strain rate, u_s is the slip velocity, which is the velocity of the fluid layer relative to the adjoining wall, and δ is the distance from the surface to the location where the boundary condition is applied, also known as the slip plane. Slip length is defined as the distance from the slip plane where the linearly extrapolated value of the velocity is equal to the velocity of the wall (zero for the case of gravity driven flows), as displayed in Fig. 1. Navier⁴³ proposed a similar form of the aforementioned slip boundary condition where the slip length depends upon the interfacial friction coefficient ζ_0 and the fluid viscosity μ_0 as $l_s = A\mu_0/\zeta_0$, where A is the interfacial area. Although significant progress has been made to understand the interfacial friction coefficient,^{44–46} the common approach is to ignore the inhomogeneity in the density and the viscosity across the confinement. Huge variations in the velocity gradient in the interfacial region can also lead to uncertainties in the computed value of slip length,⁴⁷ thereby limiting the applicability of Non-Equilibrium Molecular Dynamics (NEMD) as a reliable tool to compute slip length. An exhaustive mention of these issues is given recently by Kannam *et al.*,^{41,42} where significant differences in the reported values of slip length have been highlighted.

Recently, we have proposed a quasi-continuum model for gravity driven flow,⁴⁸ which evaluates both viscous and slip flow contributions independently and superimposes their results. Viscous contributions are incorporated by spatially

^{a)}Electronic mail: aluru@illinois.edu

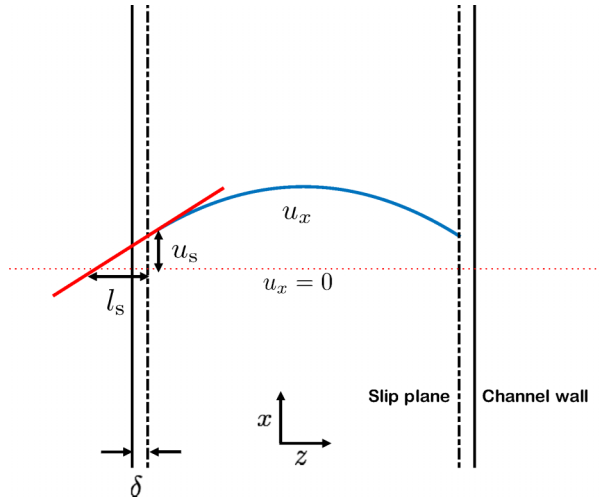


FIG. 1. Schematic plot of the 1D transport problem.

inhomogeneous density and viscosity models. The slip motion of the fluid is modeled using a static Langevin equation. The friction coefficient in the Langevin equation is obtained from Equilibrium Molecular Dynamics (EMD) simulations by computing the autocorrelation of the total wall-fluid force in the streaming direction.^{45,49} Although the methodology is tractable and provides fast and reliable results, it possesses a few shortcomings such as the *ad hoc* treatment of the location of the slip plane at the first density peak, and overlooking cases with high adsorbed density.

In this paper, we refine our existing transport model to address these limitations. We argue, in similar spirit as Huang and Szlufarska,⁵⁰ that the friction experienced by the fluid particles in the interfacial region is additive. Moreover, the motion of the fluid particles near the interface is strongly dependent on the potential energy landscape manifested by the wall structure and its interaction parameters with the fluid. Under the additional influence of thermal noise, the dynamics of a fluid particle can be accurately described by the generalized Langevin Equation (GLE). It has been shown recently that the GLE can be used to simulate the single-particle dynamical properties of confined fluids.^{51,52} Also, it has been shown that thermal noise in confined fluids can be assumed as spatially isotropic, and is not significantly different compared to the corresponding fluid in the bulk state (without the presence of confinement). With this knowledge, we discuss a novel GLE based approach to compute the correlations necessary to calculate the interfacial friction coefficient. Once the friction coefficient is known, one can obtain the slip velocity as a boundary condition, which makes the problem well-posed, and then a one-dimensional, isothermal, steady-state velocity profile can be obtained using the continuum method. The friction coefficient, therefore, serves as a bridge between the continuum and the atomistic descriptions of the transport problem.

The remainder of the paper is organized as follows: in Sec. II we present the hydrodynamic transport model. We review an empirical potential based quasi-continuum theory (EQT) to calculate the density profiles of the fluid under confinement in slit channels. To obtain local viscosity, Local Average Density Method (LADM) proposed by Bitsanis *et al.*^{29,30} is used with equation of state for shear viscosity

developed from bulk MD simulations. The slip motion is described by a GLE, as a refinement to our earlier work, which eliminates the need to perform an EMD simulation to compute the force correlations. In Sec. III, succinct details of the MD and GLE simulations are provided. In Sec. IV, results obtained from the hydrodynamical model are discussed and compared with NEMD simulations. Finally, conclusions are drawn in Sec. V.

II. TRANSPORT MODEL

The starting point of a one-dimensional gravity driven flow in a slit channel is the Stokes equation

$$\frac{d}{dz} \left[\mu(z) \frac{du_x(z)}{dz} \right] + m\rho(z)g_x = 0, \quad (2)$$

with boundary conditions

$$u_x \left(-\frac{L}{2} + \delta \right) = u_x \left(+\frac{L}{2} - \delta \right) = u_s, \quad (3)$$

where (x, z) are the streaming direction (direction of the flow) and the confined direction, respectively; $u_x(z)$ is the unknown streaming velocity, m is the molecular mass of the fluid, g_x is the applied gravity in the streaming direction, $\rho(z)$ is the number density, $\mu(z)$ is the shear viscosity, and L is the channel width. The channel walls are located at $-L/2$ and $+L/2$. Dirichlet boundary conditions are provided at a distance δ from the wall, where the first fluid layer starts to develop after the void region near the interface, with u_s as the slip velocity. The continuity equation is satisfied under the assumption that u_z is identically zero. A mathematically equivalent set of boundary conditions for the current problem can also be written as

$$A\mu(z) \frac{du_x(z)}{dz} \Big|_{z=-L/2+\delta} = \zeta_0 u_s, \quad (4a)$$

$$\frac{du_x(z)}{dz} \Big|_{z=0} = 0, \quad (4b)$$

where A is the interfacial area and ζ_0 is the macroscopic interfacial friction coefficient. Eq. (4a), although similar to the slip boundary condition presented in Eq. (1), describes the force balance at the interface. At the interface, the wall shear force is balanced by the interfacial friction force, which is proportional to the relative velocity between the wall and the fluid (slip velocity). The second condition in Eq. (4b) is representative of the symmetry of the velocity profile at the center point of the slit channel. Integrating the Stokes equation (Eq. (2)) once in the region $(-L/2 + \delta, 0)$ and using Eq. (4b), we get

$$-\mu(z) \frac{du_x(z)}{dz} \Big|_{z=-L/2+\delta} + mg_x \int_{-L/2+\delta}^0 \rho(z) dz = 0. \quad (5)$$

Now, making use of Eq. (4a) and observing that $\rho(-L/2, -L/2 + \delta) = 0$, Eq. (5) can be reformulated to obtain an expression for the slip velocity (u_s) as

$$u_s = A \frac{mg_x}{\zeta_0} \int_{-L/2}^0 \rho(z) dz. \quad (6)$$

This value of slip velocity can be used as a Dirichlet boundary condition in Eq. (3). Inputs required for this framework are density, viscosity, and the interfacial friction coefficient ζ_0 . The methods to obtain these inputs are discussed below.

A. Density profiles

We use EQT^{21–25} to compute density profiles in confined nanochannels. EQT is a continuum based multiscale formulation that can be used to obtain the density and corresponding total potential of mean force (PMF) of confined fluids in a self-consistent manner. Being a continuum approach, it is orders of magnitude faster and also comparable in accuracy with particle based sampling methods such as MD. The relevant one-dimensional (1D) density equations of EQT, for a semi-infinite slit like channel (only 1D variation along z -direction is being considered), can be written as a 1D Nernst-Planck equation

$$\frac{d}{dz} \left[\frac{d\rho(z)}{dz} + \frac{\rho(z)}{k_B T} \frac{dU^{\text{tot}}(z)}{dz} \right] = 0, \quad (7)$$

with boundary conditions and integral constraint on average channel density as

$$\rho \left(-\frac{L}{2} \right) = \rho \left(+\frac{L}{2} \right) = 0, \quad (8a)$$

$$\frac{1}{L} \int_{-L/2}^{+L/2} \rho(z) dz = \rho_{\text{avg}}. \quad (8b)$$

Here, $U^{\text{tot}}(z)$ is the total one dimensional PMF, T is the fluid temperature, k_B is the Boltzmann constant, and ρ_{avg} is the average number density of the fluid in the slit, which depends upon the thermodynamic state of the fluid, i.e., operating temperature and pressure. The total PMF (U^{tot}) has contributions from the wall-fluid (U^{wf}) and the fluid-fluid (U^{ff}) PMF, and is given by $U^{\text{tot}}(z) = U^{\text{wf}}(z) + U^{\text{ff}}(z)$. These contributions are computed separately using the interaction potentials between the particles and their densities as^{21–25}

$$U^{\text{wf}}(z) = \int_V u^{\text{wf}}(|z-r|) \rho_{\text{wall}}(r) dV, \quad (9a)$$

$$U^{\text{ff}}(z) = \int_V u^{\text{ff}}(|z-r|) \rho(r) dV, \quad (9b)$$

where u^{wf} and u^{ff} are, respectively, the continuum based pair potentials between the wall-fluid and the fluid-fluid particles, dV is the infinitesimal volume element centered at r , $\rho(r)$ is the fluid number density, and V is the cutoff volume. Development of EQT based quasi-continuum potentials is carried out using systematic coarse graining techniques of relative entropy and PMF matching, and is described in detail in Refs. 24 and 25 for Single Point Charge Extended (SPC/E) water⁵³ confined in nanochannels.

B. Viscosity profiles

Similar to our previous approach, we compute the shear viscosity of the confined fluid using the LADM.⁵⁴ It coarse-grains the local density over one molecular diameter size, and

effectively identifies a state of homogeneous fluid ($\bar{\rho}, T$), for each location z in the confinement. The 1D local average density is calculated as

$$\bar{\rho}(z) = \frac{6}{\sigma_{\text{ff}}^3} \int_{|z-z'| < \sigma_{\text{ff}}/2} \left[\left(\frac{\sigma_{\text{ff}}}{2} \right)^2 - (z-z')^2 \right] \rho(z') dz', \quad (10)$$

where σ_{ff} is the Lennard-Jones (LJ) diameter of the fluid, and for SPC/E water its value is 0.317 nm. The properties of homogeneous fluids are well understood and can easily be calculated from MD. Although equations of state for these properties exist for LJ type of fluids,^{55–57} no comprehensive database or formulae exist for the shear viscosity of bulk water. Therefore, we performed EMD simulations for bulk water and used Green-Kubo formulation to compute the shear viscosity of SPC/E water.⁵⁸ Further computational details are provided in Sec. III.

C. Interfacial friction coefficient

To compute the interfacial friction coefficient ζ_0 , we follow the linear response theory approach presented by Huang and Szlufarska in Ref. 50. We first compute the friction coefficient ζ_0^j of an individual fluid particle j near the interface. Using linear response theory in conjunction with GLE, the Green-Kubo relation for ζ_0^j can be expressed in terms of equilibrium time correlation functions as⁵⁰

$$\zeta_0^j = \frac{\int_0^\infty \langle f_{x,j}^{\text{wf}}(0) f_{x,j}^{\text{wf}}(t) \rangle dt}{k_B T + \int_0^\infty \langle v_{x,j}(0) f_{x,j}^{\text{wf}}(t) \rangle dt}, \quad (11)$$

where $f_{x,j}^{\text{wf}}$ and $v_{x,j}$ are the instantaneous streaming direction wall-fluid force and velocity of the particle j near the solid wall. The time correlation in the numerator is the single-particle wall-fluid force autocorrelation function (FACF) and denominator contains wall-fluid force–velocity cross-correlation function (FVCCF). Then, we sum the contributions from all the interfacial fluid particles to obtain the total interfacial friction coefficient ζ_0 as

$$\zeta_0 = \sum_j \zeta_0^j. \quad (12)$$

The FACF and FVCCF in Eq. (11) can be evaluated either from EMD simulation or any other particle sampling method that can simulate the single-particle dynamical motion of confined fluids in equilibrium. Once the friction coefficient is known, the slip velocity is computed from Eq. (6), thereby rendering the model closed.

In this work, we discuss a GLE based simulation approach to compute the interfacial friction coefficient. The description of a particle's motion by a GLE provides a powerful coarse-grained multiscale approach to study its equilibrium correlation functions. GLE describes the motion of a test particle in terms of dissipative and thermal forces (thermal noise), which are coupled via fluctuation-dissipation (FD) relation.^{59,60} The practical use of GLE can be made to study physical systems provided the memory function that characterizes the

dissipative force and the thermal noise autocorrelation, is known *a priori*. Sanghi and Aluru^{51,52} recently demonstrated that the thermal noise properties in confined fluids do not change significantly across the confinement. Further, thermal noise characteristics in confined fluids are not found to be significantly different than that of the same fluid in the corresponding bulk state. Therefore, the dynamics of confined fluid can be modeled using the noise characteristics of the bulk fluid; and confinement effects can be modeled by a position dependent mean force, which can be obtained from EQT. Using this GLE approach, they simulated the single-particle motion along the confined direction and computed several dynamical quantities (mean-squared displacement, survival probability, velocity autocorrelation function, etc.) at different spatial regions of confined slit channels. The computed quantities were found in good quantitative agreement with those obtained from EMD simulations. With this knowledge, to compute the interfacial friction coefficient, we formulate a two-dimensional (2D) GLE model as

$$m \frac{dv_{z,j}(t)}{dt} = -m \int_0^t K(t-t') v_{z,j}(t') dt' + f_{z,j}^{\text{tot}}(z_j(t)) + R_z(t), \quad (13a)$$

$$m \frac{dv_{x,j}(t)}{dt} = -m \int_0^t K(t-t') v_{x,j}(t') dt' + f_{x,j}^{\text{tot}}(x_j(t), z_j(t)) + R_x(t), \quad (13b)$$

$$\frac{dz_j(t)}{dt} = v_{z,j}(t), \quad \frac{dx_j(t)}{dt} = v_{x,j}(t). \quad (13c)$$

Here, m is the mass of the fluid particle j , while $v_{z,j}$, $v_{x,j}$ are, respectively, the velocities in the confined (z) and streaming (x) directions. Time dependent memory function $K(t)$ characterizes the dissipative force, $f_{z,j}^{\text{tot}}$ and $f_{x,j}^{\text{tot}}$ are the instantaneous forces in z and x directions, respectively, experienced by the particle due to the structural inhomogeneity, while $R_z(t)$ and $R_x(t)$ are the random forces in confined and streaming directions, respectively. The random force satisfies the following statistical properties:

$$\langle R_\alpha(t) \rangle = 0, \quad (14a)$$

$$\langle v_{\alpha,j}(0) R_\beta(t) \rangle = 0, \quad (14b)$$

$$\langle f_{\alpha,j}^{\text{tot}}(0) R_\beta(t) \rangle = 0, \quad (14c)$$

$$\langle R_\alpha(0) R_\beta(t) \rangle = m k_B T K(t) \delta_{\alpha\beta}, \quad (14d)$$

where α and β are the directions in the 2D system (x and z), and $\delta_{\alpha\beta}$ is the Kronecker delta, which is unity only when $\alpha = \beta$ and zero otherwise. The memory function $K(t)$ in both confined (Eq. (13a)) and streaming (Eq. (13b)) direction equations is the same. Since the memory function is same in the two directions, the thermal force also has identical statistical properties in both directions (noise is assumed isotropic, Eq. (14d)). Also, the memory function for this confined system is assumed to be the same as the memory function of the corresponding bulk water state. To justify this assumption, we compare the memory function $K(t)$ of bulk water and water confined within the first interfacial layer of $4\sigma_{\text{ff}}$ wide silicon slit channel in Fig. 2(a). The confined water is in equilibrium with bulk water

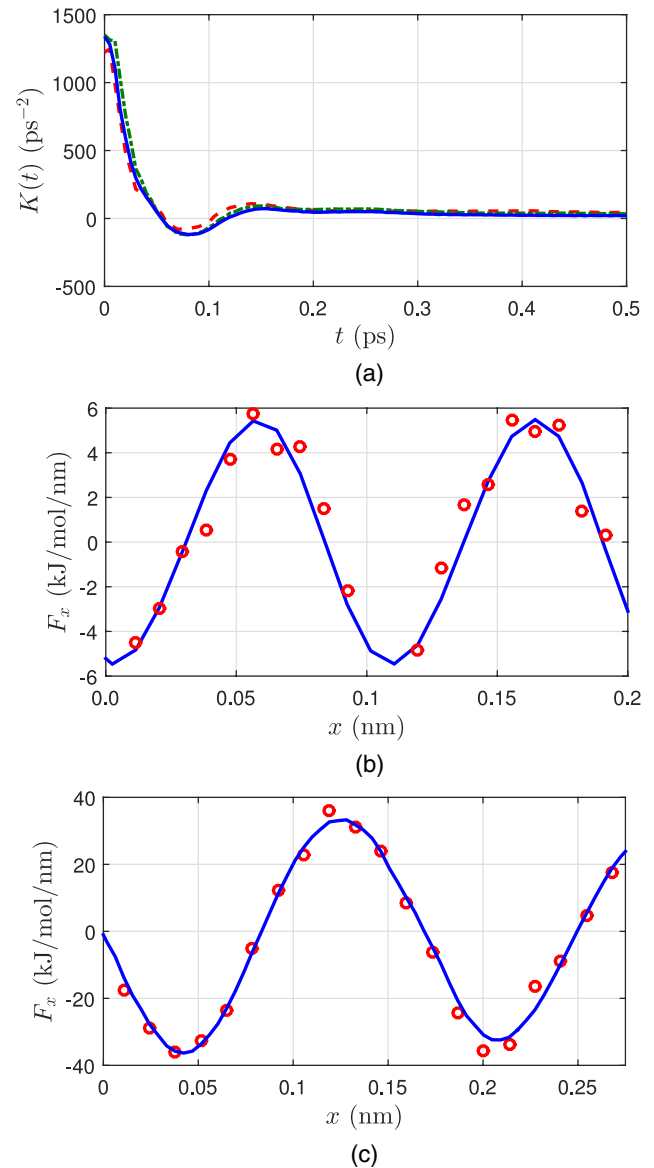


FIG. 2. (a) Memory function of SPC/E bulk water (blue line) at 298 K and density $33.46 \text{ molecules/nm}^3$. Also plotted are memory function of water in the streaming (green dashed-dotted line) and confined (red dashed line) direction for $4\sigma_{\text{ff}}$ wide silicon-water system. Mean wall-fluid (solid blue line) and total (red open circles) force in the streaming direction for (b) graphene-water, and (c) silicon-water interface.

at density $33.46 \text{ molecules/nm}^3$. It can be observed from the plot that the time decay characteristics and the correlation time of the memory function are not significantly different from corresponding bulk state even under high degree of confinement. The data for the memory function for bulk water are provided in the supplementary material.⁶¹ The instantaneous force values on particle j , i.e., $f_{z,j}^{\text{tot}}$ and $f_{x,j}^{\text{tot}}$, are realized from the static mean force maps $F_z^{\text{tot}}(z)$ and $F_x^{\text{tot}}(x, z)$. Since the magnitude of F_z^{tot} is very large near the interface, its variation along x is ignored, and it is directly obtained from EQT as $F_z^{\text{tot}}(z) = -dU^{\text{tot}}(z)/dz$. This means that the dynamics along the confined direction is primarily dictated by a 1D GLE formulation (Eq. (13a)), as demonstrated by Sanghi and Aluru.^{51,52} However, it is necessary to consider the variation of F_x^{tot} in both directions, since its variation in the streaming direction is necessary to capture the effect

of surface corrugations on the friction coefficient, and its magnitude changes very sharply along the confined direction near the interface. Also, the total mean force map along the streaming direction can be approximated as the wall-fluid force map ($F_x^{\text{tot}}(x, z) \approx F_x^{\text{wf}}(x, z)$). This approximation means that the spatial inhomogeneity in the fluid density profile in the streaming direction primarily results due to the variation in the wall-fluid potential. Figures 2(b) and 2(c) show the comparison of the streaming direction total force and the wall-fluid force profile for graphene-water and silicon-water interfaces, calculated using EMD, at the location of the first density peak. It can be observed that the wall-fluid force profile does not differ significantly from the total force profile near the interface. The advantage of this approximation is that the two-dimensional wall-fluid force map can be computed analytically using the structure of the wall as

$$U_{3D}^{\text{wf}}(x, y, z) = \sum_{r_i < R_{\text{cut}}} u_{\text{LJ}}^{\text{wf}}(r_i), \quad (15a)$$

$$\frac{dU_{3D}^{\text{wf}}}{dx} = \sum_{r_i < R_{\text{cut}}} \frac{du_{\text{LJ}}^{\text{wf}}}{dr_i} \cdot \frac{x - x_i}{r_i}, \quad (15b)$$

$$F_x^{\text{wf}}(x, z) = - \frac{\int_0^{L_y} \frac{dU_{3D}^{\text{wf}}}{dx} \exp(-\beta U_{3D}^{\text{wf}}) dy}{\int_0^{L_y} \exp(-\beta U_{3D}^{\text{wf}}) dy}, \quad (15c)$$

where $r_i = ((x - x_i)^2 + (y - y_i)^2 + (z - z_i)^2)^{1/2}$ is the distance between the wall particle centered at (x_i, y_i, z_i) to the point of interest (x, y, z) , $u_{\text{LJ}}^{\text{wf}}$ is the 12-6 LJ wall-fluid interaction potential, U_{3D}^{wf} is the three dimensional wall-fluid interaction energy, $\beta = 1/k_B T$, and L_y is the box length in the y direction. The wall particles which are inside the cutoff length $R_{\text{cut}} = 1.4$ nm are considered in the summation, similar to the confined MD simulations. Therefore, all the inputs needed to compute the interfacial friction coefficient are obtained without using computationally expensive EMD. The numerical details to solve 2D GLE model are discussed in Sec. III. We will compare the accuracy of our proposed GLE approach versus the EMD in the results section.

III. SIMULATION DETAILS

Different types of MD simulations are performed in the present work. We used the LAMMPS⁶² package in all of our computations. Water-water interactions are described by the SPC/E model.⁵³ To calculate the electrostatic interactions between water molecules, Particle-Particle Particle-Mesh (PPPM) method is used. First, EMD simulations of bulk water are performed to evaluate the shear viscosity using the Green-Kubo method as⁶³

$$\mu = \frac{V}{6k_B T} \int_0^\infty \sum_\alpha \sum_{\beta \neq \alpha} \langle P_{\alpha\beta}(0) P_{\alpha\beta}(t) \rangle dt, \quad (16)$$

where V is the volume of the simulation box, $P_{\alpha\beta}$ is the off-diagonal stress component, and α, β are the directions in the Cartesian coordinate system (x, y, z) . These computations are

performed for a range of reduced densities $\rho\sigma_{\text{ff}}^3 = 0.1-1.6$ in an NVE ensemble. After that, we computed the time autocorrelation of the off-diagonal stress components and fitted the results to a Gaussian-exponential form to capture the two stage relaxation process of the autocorrelation.⁵⁸ We used the resultant fit to compute the integral in Eq. (16). Our computed viscosity values around the state point $\rho\sigma_{\text{ff}}^3 = 1.0$ were found in good agreement (maximum 4% deviation) with the published data for SPC/E model.⁶⁴ The density versus viscosity data are then fitted to a cubic Hermite polynomial. The viscosity data along with the coefficients of the cubic Hermite polynomial are provided in the supplementary material.⁶¹ The resultant fit is then used in conjunction with LADM to estimate viscosity in the confinement by interpolation. The EMD data points and the fit are plotted in Fig. 3.

EMD simulations of confined water are performed with two different surfaces representing contrasting levels of interfacial friction. Wall-fluid interactions are modeled by the 12-6 LJ potential. The first system consists of water confined in graphene sheets at 298 K,²⁴ and serves as a low friction case. The carbon-water LJ interaction force-field is taken from Gordillo and Marti.⁶⁵ For this force-field, the interactions between the hydrogens of water and carbon are ignored. We also studied the graphene-water and graphite water systems with carbon-water interaction force-field provided by Wu and Aluru,⁶⁶ which includes carbon hydrogen interactions, and is realistic in terms of reproducing the experimental contact angle between water and graphite surface. The motivation behind the usage of different force-fields is two-fold, which is to test the fidelity of the transport model and to understand the effects of wall-fluid interaction parameters on the flow characteristics. For the second system, water is confined inside two four-layered rigid silicon walls oriented in [111] direction at 300 K,²⁵ and is representative of high friction type surface. The total number of particles in confined simulations corresponds to a reference bulk state of 33.46 molecules/nm³, and is estimated using the linear superposition approximation.^{67,68}

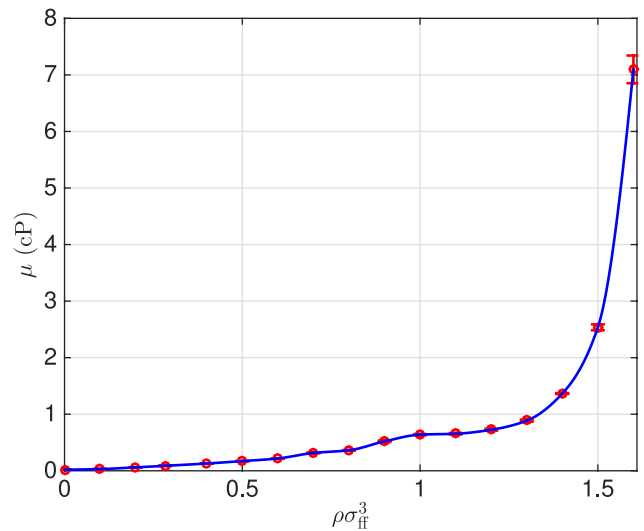


FIG. 3. Viscosity variation of SPC/E water in centipoise units (cP) with reduced density at 298 K. Open circles (red) represent EMD data points, while solid line (blue) represents cubic Hermite interpolation. Error bars in EMD data are of the size of the circles, except for $\rho\sigma_{\text{ff}}^3 = 1.6$.

Channel width is defined as the center to center distance between the first layer of wall atoms closest to the fluid. This definition is used to calculate the average channel density ρ_{avg} . The channel widths considered in this work are $20\sigma_{\text{ff}}$, $10\sigma_{\text{ff}}$, $7\sigma_{\text{ff}}$, and $4\sigma_{\text{ff}}$ to test the model accuracy for various length scales. In confined EMD simulations, systems are equilibrated for 5 ns by simulating an NVT ensemble with Nosé–Hoover thermostat⁶⁹ with a time constant of 0.2 ps. After that, production run for 10 ns is performed, with data collected every 0.02 ps for calculating the necessary correlations. These data are divided into 1000 similar samples of 10 ps, which serve as ensembles under the ergodic hypothesis, and the resultant correlations are averaged by the number of samples.

For confined NEMD simulations, different magnitudes of gravity field are considered to demonstrate the applicability of the continuum method under the linear response regime, i.e., the velocity profile scales linearly with the applied gravity, and the slip length is independent of the applied gravity.⁷⁰ To control the temperature in NEMD simulations, thermostat is only applied to non-streaming directions to prevent any artifacts in the simulation. To perform the ensemble average, 15 identical simulations are performed, differing only in their initial velocity distribution. Each ensemble is simulated for 20 ns, with first 10 ns discarded to obtain the fully developed, steady-state velocity profile.

In the transport model, the slip plane location (δ) is defined to be the distance from the surface until which the density value is less than 10^{-3} molecules/nm³. For graphene-water⁶⁵ system, this value is 0.27 nm, while for silicon-water system, it is 0.24 nm. The location of the slip plane is dependent upon the thermodynamic state and the force-fields used in the MD simulation. Density profiles are obtained from EQT and its implementation details can be found in Ref. 25. To compute the interfacial friction, 2D GLE simulations are performed with a time step of 0.01 ps, with the production trajectory of 400 ps, with data saved every other step (0.02 ps). The numerical procedure to obtain the memory function $K(t)$ and the time integration of the GLE is discussed in Ref. 52. First 100 ps of the simulation trajectory were discarded to allow the equilibration of the fluid particle. We used $\sim 2 \times 10^4$ instances of particle trajectories to compute the time correlations in Eq. (11).

A typical GLE simulation for 100 ps equilibration and 400 ps production run takes about 144 s in central processing unit (CPU) time. In contrast, a typical EMD simulation is orders of magnitude slower (approximately 24 CPU hours to simulate a 500 ps run for graphene water $10\sigma_{\text{ff}}$ system). Also, as GLE is a single particle formulation, it can be run on a personal workstation, as opposed to EMD/NEMD, which requires suitable parallelization and high performance

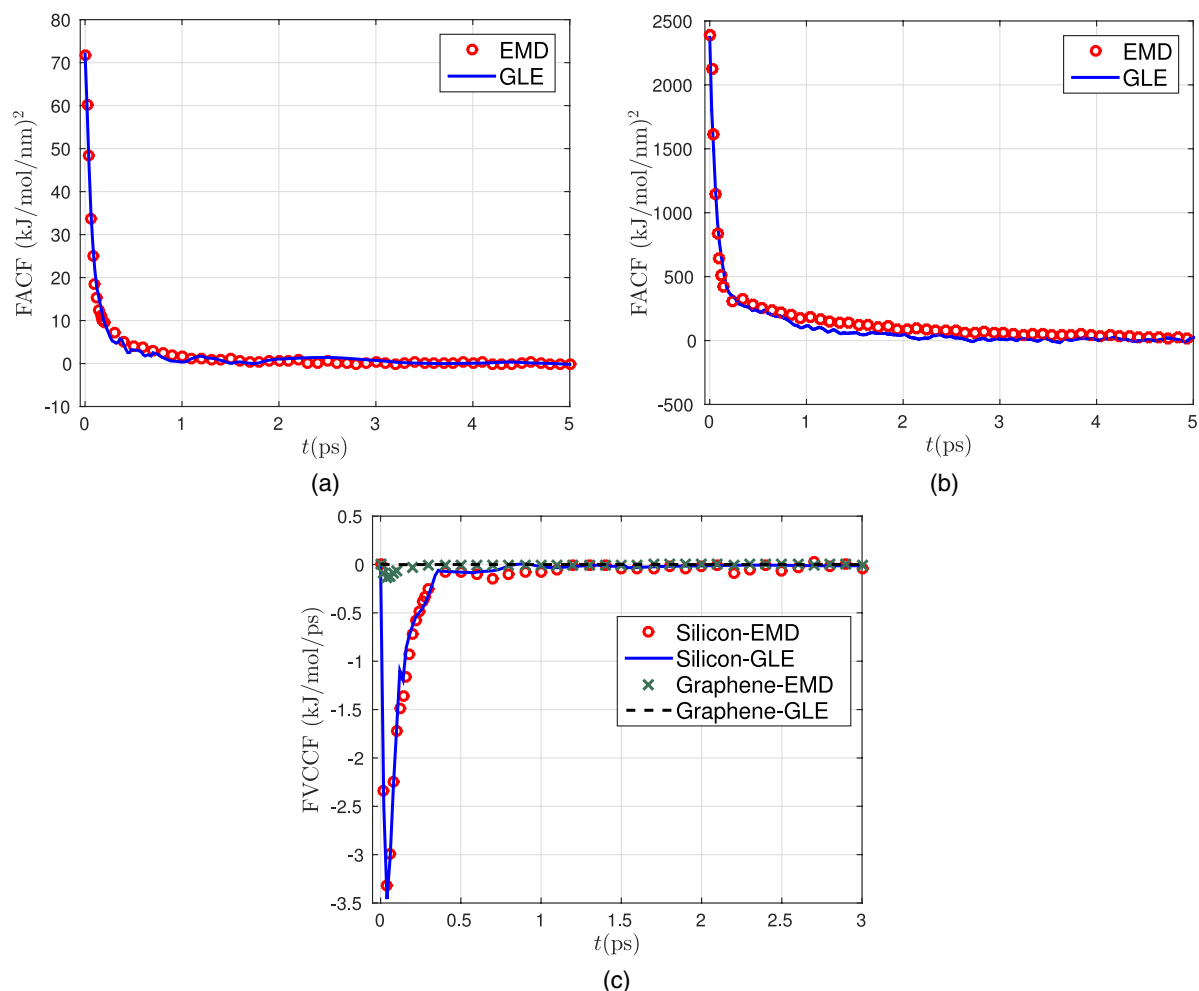


FIG. 4. Wall-fluid FVCCF from GLE (bold line, blue) and EMD (circles, red) for (a) graphene-water⁶⁵ and (b) silicon-water interfaces. (c) FVCCF from GLE and EMD for water with graphene and silicon interfaces.

TABLE I. Friction coefficient ζ_0 (kJ-ps/mol/nm²).

Surface	EMD	GLE
Graphene water ⁶⁵	123.73	125.14
Silicon water	4.05×10^4	3.93×10^4

computing cluster environments to reduce the walltime. The continuum formulation typically takes 3-4 s as compared to NEMD, where meaningful data for velocity profiles require 53 350 CPU hours of production runs. Therefore, our GLE/continuum framework provides a massive speedup over NEMD to obtain the velocity profiles.

IV. RESULTS

In this section, we test the efficacy of the current framework by comparing the velocity profiles predicted from the model with those obtained from NEMD simulations. We also compare the accuracy of the correlation functions obtained using the proposed GLE approach with the EMD results. For EMD calculations of the friction coefficient, a perpendicular distance of $1\sigma_{ff}$ from the wall in the confined direction is chosen as cutoff distance, and the region between the wall

and the cutoff distance is defined as interfacial region. Initial time occupancy based tagging^{51,71} is used to compute the time correlations. This means that only the particles that are present in the interfacial region at an initial time contribute to the interfacial friction. This is done because for large cutoff lengths, the friction coefficient will include both the viscous and the slip effects and therefore will not remain an intrinsic property of the wall-fluid interface, as assumed in the formulation. This point has been discussed in detail by Hansen *et al.*⁴⁴ Also, Huang and Szlufarska⁵⁰ have acknowledged the issue, and have verified the formulation by computing the friction coefficient inside 2 molecular diameter wide channel, where the entire body of the fluid becomes a wall-fluid interface. In GLE, the single particle friction is multiplied by the average number of particles in the cutoff region instead of the summation, which is obtained from the 1D density profiles. We show the comparison of the single-particle FACS calculated from EMD and GLE formulations for graphene⁶⁵ and silicon walls in Figs. 4(a) and 4(b), respectively. It can be observed from these figures that the correlations computed from the GLE trajectories are in good quantitative agreement to their EMD counterpart. Silicon interface offers higher friction than graphene,⁴⁸ which is clearly evident from the FACS plots where its variance is significantly higher in the case of silicon.

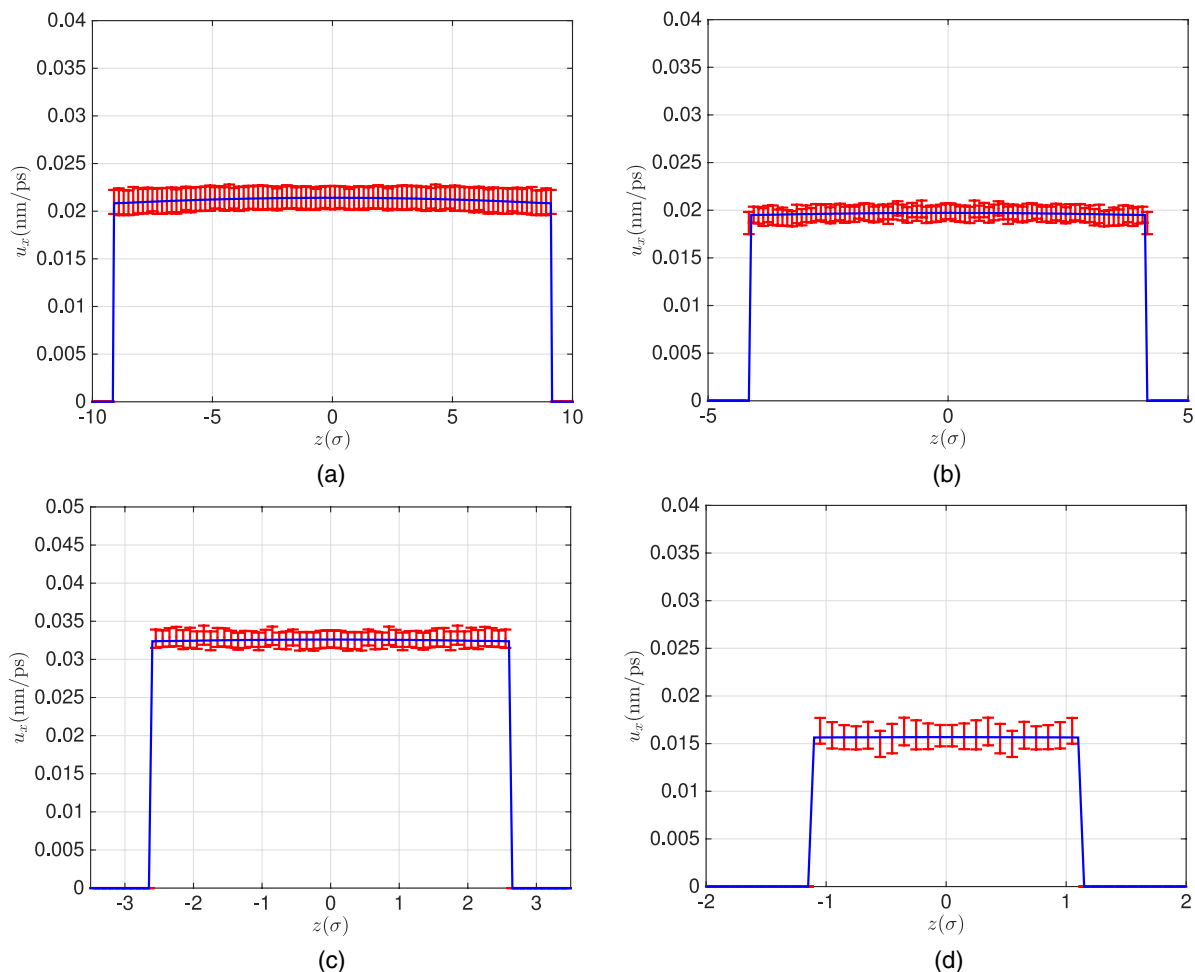


FIG. 5. Velocity profiles of water in graphene slits of size (a) $20\sigma_{ff}$ for $g_x = 1 \times 10^{-4}$ nm/ps², (b) $10\sigma_{ff}$ for $g_x = 2 \times 10^{-4}$ nm/ps², (c) $7\sigma_{ff}$ for $g_x = 5 \times 10^{-4}$ nm/ps², and (d) $4\sigma_{ff}$ for $g_x = 5 \times 10^{-4}$ nm/ps² using force-field of carbon-water from Gordillo and Marti.⁶⁵ Continuum results are in solid line (blue), while MD results are represented by error bars (red).

Figure 4(c) displays the comparison of the FVCCF for the two interfaces as obtained from GLE and EMD simulations. It can be observed from the plot that the silicon interface presents a strong short-time force–velocity cross-correlation which is captured accurately by GLE based dynamics. However, the FVCCF for graphene water interface is almost negligible. As a result, the contribution to the friction coefficient from the FVCCF term is only significant (in comparison to the thermal energy $k_B T \approx 2.5$ kJ/mol) for the silicon interface (with integral value -0.536 kJ/mol), as compared to graphene interface (with integral value -0.018 kJ/mol). The reason for this difference can be understood from Figs. 2(b) and 2(c), which show the variation of the streaming direction wall–fluid force for the two interfaces. It can be observed that both the magnitude and the period of the wall–fluid force is smaller for graphene in comparison to silicon, leading to a very small residence time of the water molecule near the graphene interface (~ 0.2 ps). Therefore, the motion of water molecule in the streaming direction for graphene interface is thermal noise dominant, giving rise to a significantly smaller contribution to the FVCCF. Table I shows the comparison of the friction coefficient computed using the GLE approach with those obtained from EMD simulations. Assuming the EMD value as a benchmark, the deviation in the friction coefficient

calculated from the GLE is within 3%. Thus, the proposed GLE formulation provides a robust and computationally efficient alternative to compute the interfacial friction.

To compare the accuracy of our transport model, NEMD simulations of confined water in graphene and silicon surfaces are used as a benchmark. Using our approach, we first seek to address the important question of relative contributions of viscous and slip flow in the velocity profile. After the friction coefficient is calculated, we compute the slip velocity u_s by using Eq. (6) and solve the transport model. As expected, smooth surfaces (low interfacial friction) will enhance the relative motion between the wall and the adjoining fluid layer, rendering slip as the dominant transport mechanism. This is reflected in the plug-like velocity profiles of water in graphene nanochannels as shown in Figs. 5(a)–5(d). For atomistically rough surfaces (high interfacial friction), such as water confined within silicon walls, the role of viscosity becomes more important as seen from Figs. 6(a)–6(d). Increased corrugations on silicon surface hinder the motion of adjacent fluid layer considerably, and transport is dominated by viscous flow. Density and viscosity variations in the current framework capture the non-parabolic velocity profiles, which are more pronounced near the interface and can be seen clearly in narrower channels such as $7\sigma_{ff}$ (Fig. 6(c)) and $4\sigma_{ff}$

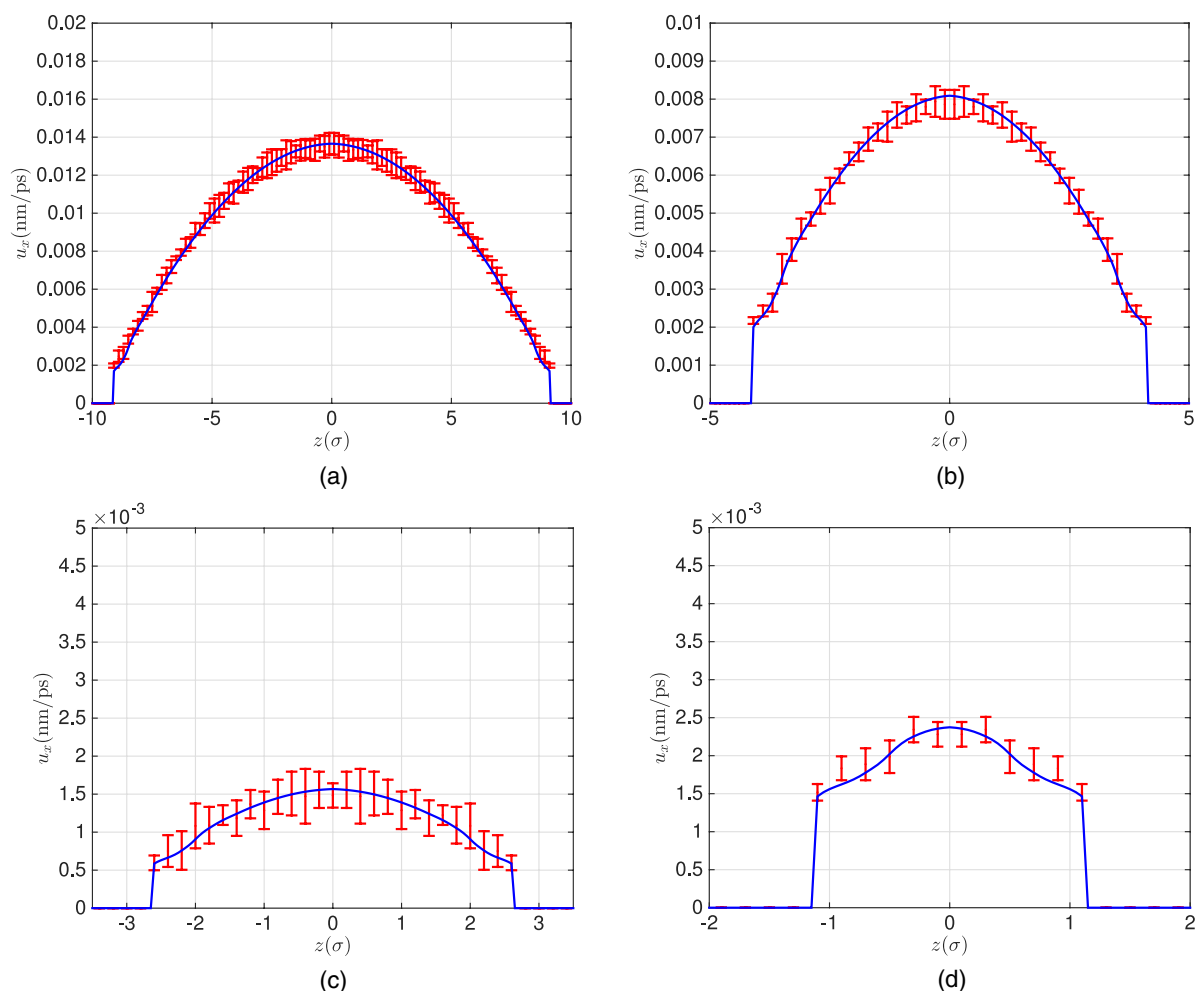


FIG. 6. Velocity profiles of water in silicon slits of size (a) $20\sigma_{ff}$ for $g_x = 2 \times 10^{-3}$ nm/ps², (b) $10\sigma_{ff}$ for $g_x = 5 \times 10^{-3}$ nm/ps², (c) $7\sigma_{ff}$ for $g_x = 2 \times 10^{-3}$ nm/ps², and (d) $4\sigma_{ff}$ for $g_x = 5 \times 10^{-3}$ nm/ps². Continuum results are in solid line (blue), while MD results are represented by error bars (red).

TABLE II. Slip lengths (nm) of water on different interfaces. CVG is an abbreviation for Continuum Velocity Gradient method (Eq. (1)), and EMD value is computed using $l_s = A\mu(-L/2 + \delta)/\zeta_0$.

System	$20\sigma_{ff}$		$10\sigma_{ff}$		$7\sigma_{ff}$		$4\sigma_{ff}$	
	CVG	EMD	CVG	EMD	CVG	EMD	CVG	EMD
Graphene ⁶⁵	44.52	45.19	44.50	45.19	44.47	45.19	44.60	45.27
Silicon	0.33	0.32	0.33	0.32	0.33	0.32	0.36	0.34
Graphene ⁶⁶	31.32	31.77
Graphite ⁶⁶	26.31	26.69

(Fig. 6(d)). It can also be observed that for $4\sigma_{ff}$ wide channel, significant velocity gradient reversals are present in NEMD profile, which are not captured accurately using the LADM calculated viscosity. For smaller channels with dominant viscous contributions, the use of LADM to capture non-local effects of viscosity might not suffice. In such instances, a transport model with strict non-local constitutive relationship between the stress and strain rate can be utilized to rectify these discrepancies.^{26,27,72,73} Approximating density and viscosity as a constant value would fail to capture this non-parabolic behavior, and therefore should be avoided.

We computed the slip length l_s using the velocity profiles obtained from the continuum model, defined through Eq. (1) for graphene (from force-fields of Gordillo and Marti⁶⁵) and silicon, and report these values in Table II. We also compare these values to the one obtained from EMD method. We observe that the computed slip length is nearly constant for a specific liquid-solid interface at a particular thermodynamic state. This observation can be utilized to identify slip length as a single parameter capable of characterizing the surface-fluid transport properties. The value of slip length of water on graphene surface is in accordance with the previous findings summarized by Kannam *et al.* in Table I of Ref. 42. Using the force-field provided by Wu and Aluru,⁶⁶ it is observed that the slip length decreases from 45 nm to 32 nm ($\zeta_0 = 180.26$ kJ-ps/mol nm²) for the graphene-water interface. This is due to the increased hydrophilic nature of the interaction parameters resulting in higher interfacial

friction, and is clear from Fig. 7(a), where the same value of applied gravity (10^{-4} nm/ps²) in $20\sigma_{ff}$ channel yields a smaller value of slip velocity (compare to Fig. 5(a)). The slip length further decreases to 27 nm ($\zeta_0 = 221.79$ kJ-ps/mol nm²) for graphite water interface (see Fig. 7(b) for velocity profile), owing to the increased attraction between the wall and the fluid due to the addition of an extra wall layer. Based on these observations, we conclude that the wall-fluid interaction parameters significantly affect the slip length and the velocity profile, and the proposed interfacial friction based model is able to capture this phenomenon with high fidelity.

Contrary to our findings, there are studies^{41,44,74} that report slip length dependence on channel width, which saturates to a constant slip length value for channel widths greater than $20\sigma_{ff}$. We interpret that these findings might stem from treatment of the problem keeping the pore average density ρ_{avg} as a constant while varying the channel width, which changes the thermodynamic state of the fluid across the channels. We argue that the slip length would remain constant when the following conditions are met:

1. The thermodynamic state of the fluid inside the channels is consistent, i.e., the chemical potential across the confinement is constant for all channel widths.
2. Density and viscosity variations are accounted appropriately in the transport model.
3. The applied gravity value does not drive the flow out of the linear response regime.⁷⁰

In addition to the above requirements, caution must be exercised while studying very small channel widths. A typical limit on the applicability of our method would be the cases where the wall-fluid potentials from the two confining walls overlap considerably. As discussed in detail by Anil Kumar and Bhatia in Ref. 75, when the channel width is decreased, the wall-fluid potential well becomes deeper to a minimum, after which it rises again. A so called ‘‘levitation effect’’ occurs at the transition point, where the assistance to the transport is maximum, i.e., the fluid particle achieves super-mobility. Below this critical size of the channel, the particle motion is hindered. A rough estimate of this critical

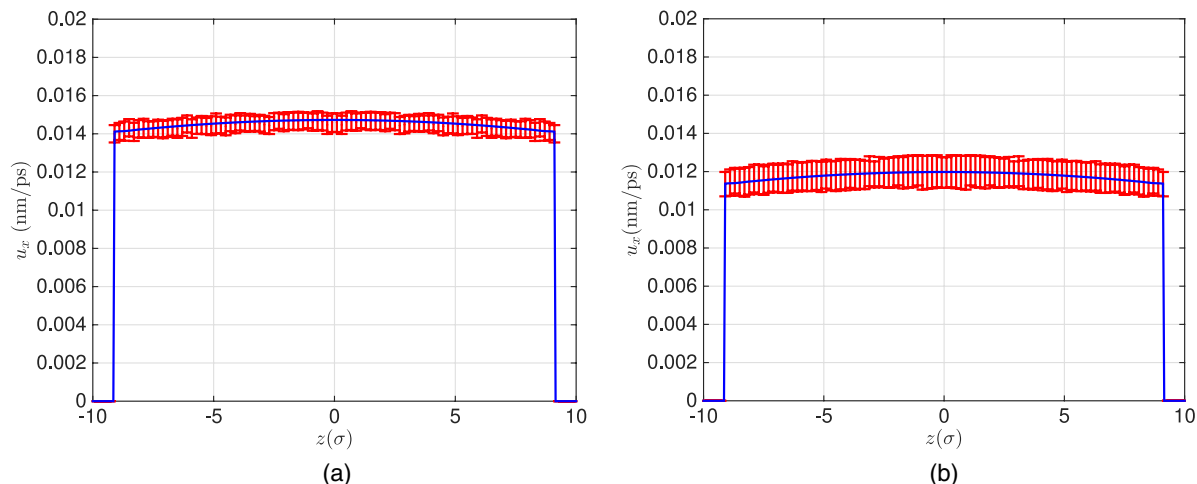


FIG. 7. Velocity profiles of water in $20\sigma_{ff}$ wide (a) graphene and (b) graphite slits using force-field of carbon-water from Wu and Aluru,⁶⁶ for $g_x = 10^{-4}$ nm/ps². Continuum results are in solid line (blue), while MD results are represented by error bars (red).

dimension neglecting the effects of kinetic energy is given as $L \sim 2(2^{1/6})\sigma_{wf}$. Since the channel widths considered here are above this critical dimension, we have not observed this effect in the present study.

V. CONCLUSIONS

In this study, we have developed a continuum based hydrodynamic transport model for gravity driven flow of water in slit shaped nanochannels. Viscous contributions are modeled by density dependent viscosity, which is evaluated using LADM. The boundary condition is provided in the form of a slip velocity, which is dependent on the interfacial friction coefficient. The friction coefficient provides the atomistic to continuum bridge by incorporating the effect of the lattice structure and the nature of wall-fluid interactions. It is estimated using the wall-fluid force autocorrelation and force-velocity cross-correlation functions, which are computed using a GLE based dynamical framework. The correlations computed using the GLE model are in good agreement with those computed using EMD simulations of confined fluid. Under application of gravity, the competing nature of viscous and slip components in fluid flow leads to different nature of velocity profiles, covering the entire spectrum from slip dominant plug like flows in smooth surfaces to viscosity dominant stick type flows in rough and high friction surfaces. Density and viscosity variations are mandatory to capture the non-parabolic nature of velocity profiles in the interfacial region. Furthermore, it is revealed from the velocity profiles that the slip length is invariant with channel width under certain conditions, and therefore it can serve as the single transport parameter characterizing the surface-fluid interaction for a fixed thermodynamic state. The proposed framework by construction embeds the nanoscale physics and yields atomistic scale accurate results with continuum scale efficiency.

ACKNOWLEDGMENTS

This work was supported by AFOSR (Grant No. FA9550-12-1-0464) and by NSF (Grant Nos. 1264282, 1420882, and 1506619). R.B. thanks Sikandar Mashayak and Kumar Kunal for helpful discussions on EQT and GLE. The authors acknowledge the use of the Taub cluster provided by the Computational Science and Engineering Program at the University of Illinois.

- ¹E. Tajkhorshid, P. Nollert, M. O. Jensen, L. J. W. Miercke, J. O'Connell, R. M. Stroud, and K. Schulten, *Science* **296**, 525 (2002).
- ²A. Barati Farimani, N. R. Aluru, and E. Tajkhorshid, *Appl. Phys. Lett.* **105**, 083702 (2014).
- ³M. Majumder, N. Chopra, R. Andrews, and B. Hinds, *Nature* **438**, 930 (2005).
- ⁴Y. Zhu and S. Granick, *Phys. Rev. Lett.* **87**, 096105 (2001).
- ⁵A. Maali, T. Cohen-Bouhacina, and H. Kellay, *Appl. Phys. Lett.* **92**, 053101 (2008).
- ⁶J. K. Holt, H. G. Park, Y. Wang, M. Stadermann, A. B. Artyukhin, C. P. Grigoropoulos, A. Noy, and O. Bakajin, *Science* **312**, 1034 (2006).
- ⁷J. A. Thomas and A. J. H. McGaughey, *Nano Lett.* **8**, 2788 (2008).
- ⁸G. Hummer, J. Rasaiah, and J. Noworyta, *Nature* **414**, 188 (2001).
- ⁹A. Kalra, S. Garde, and G. Hummer, *Proc. Natl. Acad. Sci. U. S. A.* **100**, 10175 (2003).

- ¹⁰S. Joseph and N. R. Aluru, *Phys. Rev. Lett.* **101**, 064502 (2008).
- ¹¹S. Joseph and N. R. Aluru, *Nano Lett.* **8**, 452 (2008).
- ¹²M. A. Shannon, P. W. Bohn, M. Elimelech, J. G. Georgiadis, B. J. Marinas, and A. M. Mayes, *Nature* **452**, 301 (2008).
- ¹³M. E. Suk, A. V. Raghunathan, and N. R. Aluru, *Appl. Phys. Lett.* **92**, 133120 (2008).
- ¹⁴M. E. Suk and N. R. Aluru, *J. Phys. Chem. Lett.* **1**, 1590 (2010).
- ¹⁵M. S. P. Sansom and P. C. Biggin, *Nature* **414**, 156 (2001).
- ¹⁶H. G. Park and Y. Jung, *Chem. Soc. Rev.* **43**, 565 (2014).
- ¹⁷S. K. Bhatia, M. R. Bonilla, and D. Nicholson, *Phys. Chem. Chem. Phys.* **13**, 15350 (2011).
- ¹⁸C. Neto, D. R. Evans, E. Bonaccorso, H.-J. Butt, and V. S. J. Craig, *Rep. Prog. Phys.* **68**, 2859 (2005).
- ¹⁹L. Bocquet and J.-L. Barrat, *Soft Matter* **3**, 685 (2007).
- ²⁰B.-Y. Cao, J. Sun, M. Chen, and Z.-Y. Guo, *Int. J. Mol. Sci.* **10**, 4638 (2009).
- ²¹A. V. Raghunathan, J. H. Park, and N. R. Aluru, *J. Chem. Phys.* **127**, 174701 (2007).
- ²²T. Sanghi and N. R. Aluru, *J. Chem. Phys.* **132**, 044703 (2010).
- ²³T. Sanghi and N. R. Aluru, *J. Chem. Phys.* **136**, 024102 (2012).
- ²⁴S. Y. Mashayak and N. R. Aluru, *J. Chem. Phys.* **137**, 214707 (2012).
- ²⁵S. Y. Mashayak and N. R. Aluru, *J. Chem. Theory Comput.* **8**, 1828 (2012).
- ²⁶B. D. Todd and J. S. Hansen, *Phys. Rev. E* **78**, 051202 (2008).
- ²⁷B. D. Todd, J. S. Hansen, and P. J. Davis, *Phys. Rev. Lett.* **100**, 195901 (2008).
- ²⁸K. P. Travis, B. D. Todd, and D. J. Evans, *Phys. Rev. E* **55**, 4288 (1997).
- ²⁹I. Bitsanis, J. J. Magda, M. Tirrell, and H. T. Davis, *J. Chem. Phys.* **87**, 1733 (1987).
- ³⁰I. Bitsanis, T. K. Vanderlick, M. Tirrell, and H. T. Davis, *J. Chem. Phys.* **89**, 3152 (1988).
- ³¹S. K. Bhatia and D. Nicholson, *AIChE J.* **52**, 29 (2006).
- ³²X. Gao, J. C. D. da Costa, and S. K. Bhatia, *J. Membr. Sci.* **460**, 46 (2014).
- ³³X. Yong and L. Zhang, *Microfluid. Nanofluid.* **14**, 299 (2012).
- ³⁴A. Martini, A. Roxin, R. Q. Snurr, Q. Wang, and S. Lichter, *J. Fluid Mech.* **600**, 257 (2008).
- ³⁵F.-C. Wang and Y.-P. Zhao, *Soft Matter* **7**, 8628 (2011).
- ³⁶S. K. Bhatia and D. Nicholson, *Langmuir* **29**, 14519 (2013).
- ³⁷O. G. Jepps, S. K. Bhatia, and D. J. Searles, *Phys. Rev. Lett.* **91**, 126102 (2003).
- ³⁸O. G. Jepps, S. K. Bhatia, and D. J. Searles, *J. Chem. Phys.* **120**, 5396 (2004).
- ³⁹S. K. Bhatia, O. Jepps, and D. Nicholson, *J. Chem. Phys.* **120**, 4472 (2004).
- ⁴⁰S. K. Bhatia and D. Nicholson, *J. Chem. Phys.* **127**, 124701 (2007).
- ⁴¹S. K. Kannam, B. D. Todd, J. S. Hansen, and P. J. Davis, *J. Chem. Phys.* **136**, 024705 (2012).
- ⁴²S. K. Kannam, B. D. Todd, J. S. Hansen, and P. J. Davis, *J. Chem. Phys.* **138**, 094701 (2013).
- ⁴³C. Navier, *Mém. l'Acad. R. Sci. l'Inst. France* **6**, 389 (1823).
- ⁴⁴J. S. Hansen, B. D. Todd, and P. J. Davis, *Phys. Rev. E* **84**, 016313 (2011).
- ⁴⁵L. Bocquet and J.-L. Barrat, *Phys. Rev. E* **49**, 3079 (1994).
- ⁴⁶J. Petrávic and P. Harrowell, *J. Chem. Phys.* **127**, 174706 (2007).
- ⁴⁷E. M. Kotsalis, "Multiscale modeling and simulation of fullerenes in liquids," Ph.D. thesis, ETH Zürich, 2008.
- ⁴⁸R. Bhadauria and N. R. Aluru, *J. Chem. Phys.* **139**, 074109 (2013).
- ⁴⁹J.-L. Barrat and L. Bocquet, *Faraday Discuss.* **112**, 119 (1999).
- ⁵⁰K. Huang and I. Szlufarska, *Phys. Rev. E* **89**, 032119 (2014).
- ⁵¹T. Sanghi and N. R. Aluru, *J. Chem. Phys.* **138**, 124109 (2013).
- ⁵²T. Sanghi and N. R. Aluru, *J. Chem. Phys.* **141**, 174707 (2014).
- ⁵³H. J. C. Berendsen, J. R. Grigera, and T. P. Straatsma, *J. Phys. Chem.* **91**, 6269 (1987).
- ⁵⁴T. K. Vanderlick, L. E. Scriven, and H. T. Davis, *J. Chem. Phys.* **90**, 2422 (1989).
- ⁵⁵T. H. Chung, M. Ajlan, L. L. Lee, and K. E. Starling, *Ind. Eng. Chem. Res.* **27**, 671 (1988).
- ⁵⁶N. Mehdipour and H. Eslami, *Int. J. Therm. Sci.* **41**, 949 (2002).
- ⁵⁷L. V. Woodcock, *AIChE J.* **52**, 438 (2006).
- ⁵⁸G. S. Fanourgakis, J. S. Medina, and R. Prosimiti, *J. Phys. Chem. A* **116**, 2564 (2012).
- ⁵⁹B. J. Berne and G. D. Harp, *On the Calculation of Time Correlation Functions* (John Wiley & Sons, Inc., 2007), pp. 63–227.
- ⁶⁰J. P. Boon and S. Yip, *Molecular Hydrodynamics* (McGraw-Hill, New York, London, 1980).
- ⁶¹See supplementary material at <http://dx.doi.org/10.1063/1.4934678> for the memory function and viscosity of SPC/E water at 298 K.
- ⁶²S. Plimpton, *J. Comput. Phys.* **117**, 1 (1995).

- ⁶³E. Helfand, *Phys. Rev.* **119**, 1 (1960).
- ⁶⁴S. Balasubramanian, C. J. Mundy, and M. L. Klein, *J. Chem. Phys.* **105**, 11190 (1996).
- ⁶⁵M. Gordillo and J. Marti, *Chem. Phys. Lett.* **329**, 341 (2000).
- ⁶⁶Y. Wu and N. R. Aluru, *J. Phys. Chem. B* **117**, 8802 (2013).
- ⁶⁷I. K. Snook and W. van Megen, *J. Chem. Soc., Faraday Trans. 2* **77**, 181 (1981).
- ⁶⁸S. K. Das, M. M. Sharma, and R. S. Schechter, *J. Phys. Chem.* **100**, 7122 (1996).
- ⁶⁹S. Nosé, *J. Chem. Phys.* **81**, 511 (1984).
- ⁷⁰P. A. Thompson and S. M. Troian, *Nature* **389**, 360 (1997).
- ⁷¹E. R. Pinnick, S. Erramilli, and F. Wang, *Mol. Phys.* **108**, 2027 (2010).
- ⁷²K. S. Glavatskiy, B. A. Dalton, P. J. Daivis, and B. D. Todd, *Phys. Rev. E* **91**, 062132 (2015).
- ⁷³B. A. Dalton, K. S. Glavatskiy, P. J. Daivis, and B. D. Todd, *Phys. Rev. E* **92**, 012108 (2015).
- ⁷⁴V. P. Sokhan and N. Quirke, *Phys. Rev. E* **78**, 015301 (2008).
- ⁷⁵A. V. Anil Kumar and S. K. Bhatia, *J. Phys. Chem. B* **110**, 3109 (2006).